Nanoscale Advances

ROYAL SOCIETY OF CHEMISTRY

MINIREVIEW

View Article Online
View Journal | View Issue

Cite this: *Nanoscale Adv.*, 2022, **4**, 2077

Recent advances in metal–organic frameworks for gas adsorption/separation

Chuanhai Jiang, Xiaokang Wang, Yuguo Ouyang, Kebin Lu, Weifeng Jiang, Huakai Xu, Xiaofei Wei, Zhifei Wang, Fangna Dai * and Daofeng Sun

The unique structural advantage of metal–organic frameworks (MOFs) determines the great prospect and developability in gas adsorption and separation. Both ligand design and microporous engineering based on crystal structure are significant lever for coping with new application exploration and requirements. Focusing on the designable pore and modifiable frameworks of MOFs, this review discussed the recent advances in the field of gas adsorption and separation, and analyzed the host–guest interaction, structure–performance relations, and the adsorption/separation mechanism from ligand design, skeleton optimization, metal node regulation, and active sites construction. Based on the function-oriented perspective, we summarized the main research recently, and made an outlook based on the focus of microporous MOFs that require further attention in the structure design and industrial application.

Received 25th January 2022
Accepted 22nd March 2022

DOI: 10.1039/d2na00061j

rsc.li/nanoscale-advances

1. Introduction

Metal–organic frameworks (MOFs) are organic–inorganic hybrid crystalline porous materials assembled by organic bridging linker and metal ions/cluster.[1] Since the first MOF was reported by Yaghi in 1995,[2] numerous MOF materials have been widely researched in the past decades.[3] As typical porous materials, the obvious features of MOFs are ultra-high specific surface area, permanent porosity, designable structure, tunable pore size, *etc.*,[4] which have encouraged researchers to explore their application continuously. Compared with other porous solid materials, MOFs can better highlight the controllable continuity from design to structure and performance. At present, the application fields of MOFs contain gas adsorption/separation, luminescence, sensing, catalysis, and drug delivery.[5–9] Gas adsorption and separation are considered as one of the earliest and most extensive application for MOFs, and a lot of excellent research works have been reported in the past decades (Fig. 1).[10–16] Due to the multifunctional and ever-increasing demands, it is really wise to further focus on exploring structure–performance connection of MOFs by combining diversified strategies.

Gas adsorption, such as gas storage or removal, is one of the application to reflect the pore characteristics and advantages for MOFs maximally.[17] With the development of science and technology, an urgent issue is that on the one hand, we need to seek ideal materials for storing fuel gas such as H_2 and CH_4,[18] and on the other hand, it is essential to find efficient and economical

School of Materials Science and Engineering, College of Science, China University of Petroleum (East China), Qingdao, Shandong, 266580, China. E-mail: fndai@upc.edu.cn

Chuanhai Jiang received his B.S. degree from Ludong University in 2020. Currently, He is studying for a Master's degree in China University of Petroleum (East China). His research interests focus on metal–organic frameworks and their application in gas adsorption and separation.

Fangna Dai received her PhD degree from the Shandong University. From 2017 to 2018, she was engaged in research as a visiting scholar at the Nanyang Technological University, Singapore. She is now a professor of China University of Petroleum (East China). Her research interests are in the assembly of 2D metal–organic framework and the application of gas adsorption and separation.

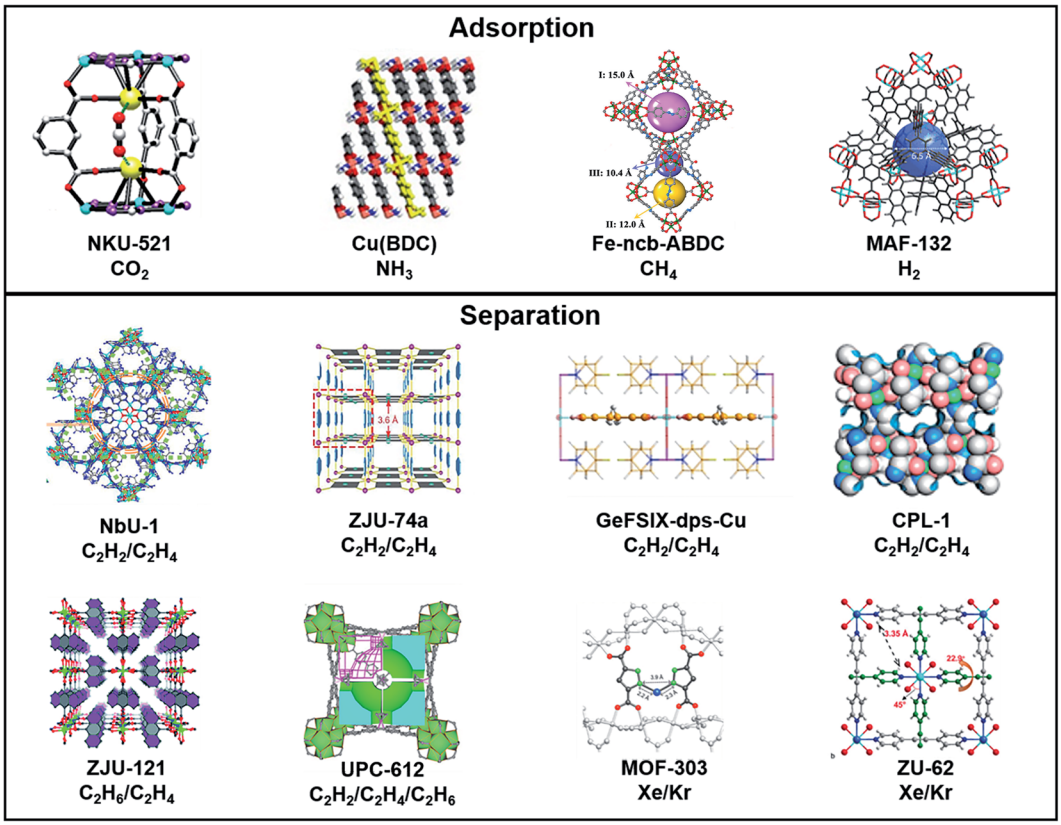

Fig. 1 Some representative MOFs for gas adsorption/separation recently.

adsorbents to removal harmful gas such as SO_2, NH_3, and CO.[19–24] MOFs are always promising candidates for gas adsorption due to the precise micropore engineering design. Generally, it is easier to meet the custom-made demands *via* precise structural adjustments. As the main place, the operation of the pore provides greater potential for binding guest molecules. For different guest molecules, targeted measures are taken to regulate the pore environment.[25] For instance, introducing functional sites into the skeleton or pores can increase the binding force between the guest and the frameworks.[26] Lewis basic N-sites can enhance the interaction between gas and networks, thus improving the ability of the gas storage.[27] Besides, a notable strategy is to produce open metal sites (OMS) by removing coordinated solvent molecules under negative pressure.[28]

Separation is an indispensable process in the industry, and the significance of gas separation is self-evident. Usually, in the chemical industry field, cryogenic distillation is an effective process for separating gas mixtures.[29] However, as an environment- and energy-intensive process, the multiple evaporation–condensation cycles would inevitably cause the waste of energy and resources.[30] It is worthy to explore the adsorbents with high adsorption capacity and separation efficiency. MOFs are considered as potential materials for gas separation due to functionalized interface, designable structure, and atom-level control.[31] According to the molecular features, a series of measures, such as ligand size adjustment,[32] ligand modification,[33] secondary building unit (SBU) modification,[34] and pore space partition,[35] are applied to adjust the pore and network environment. Based on these, identifying and magnifying the slight difference between two or three kinds molecules are the key to optimize the host–guest interactions. In contrast, the traditional solid state absorbents (*e.g.*, zeolite, molecular sieve, and porous carbon) do not show the notable advantages above.[36] Generally, the evaluation of the adsorption/separation performance is mainly as follows: the adsorption capacity is a parameter that directly reflects the working capacity, adsorption enthalpy (Q_{st}) represents the enthalpy changes due to the adsorption process, ideal adsorbed solution theory (IAST) is usually the theoretical basis for evaluating the separation potential, and the breakthrough curves obtained from the breakthrough experiments are used to demonstrate the actual separation behavior of mixed gases. Based on the above parameters, we can effectively analyze the adsorption and separation performance of MOFs.

So far, MOF materials have made diversified progress from the original research on the single structure study to the function-oriented construction. Herein, we summarize the relevant studies on MOFs in gas adsorption and separation, and present the issues needed to be focused on. Finally, we look ahead at the prospects in both new MOFs development and its practical application.

2. Gas adsorption and storage

As typical porous materials, MOFs have unique advantage to bring into play gas adsorption performance by material genes editing, post-modification, *etc.* The pore structure and controllable size of the MOFs decide the potential of high adsorption capacity, and show application prospects in improving the separation effect and reducing the energy consumption. Thus, MOFs are considered as idealized candidates for gas adsorption and storage.[37] In order to meet the actual demands, a typical vision is to achieve the selective adsorption of certain guests by diverse strategies. At present, a several MOFs have been proven to be able to achieve gas adsorption including the greenhouse and toxic gases (CO_2,[21,22] NO_x,[20] SO_2,[23,24] NH_3,[19] *etc.*) and the energy gases (H_2, CH_4, *etc.*).[18]

2.1 Greenhouse and toxic gas removal

Greenhouse gases such as CO_2 are causing global climate warming, which compels the exploration of new materials that can reduce the excess CO_2 and relieve the climate problems.[38] The combination of gas and adsorbents is based on the force between the guests and the binding site. Thus, Bu *et al.* explored MOFs with unsaturated alkali metal sites by introducing tetrazole.[39] In this work, K^+ are installed in the trinuclear Co^{2+}-tetrazole unit in NKU-521 ($[Co_3K_2(TZIA)_3(H_2O)_3](DMA)$), the active K^+ sites are fully exposed, and show CO_2 trapping after removing the coordinated H_2O molecules (Fig. 2). In the process of CO_2 capture, K^+ is considered to promote the combination of gas molecules and skeleton, which increases the isosteric heat of NKU-521a (removing the solvent molecules of NKU-521) by 24%, reaching 41 kJ mol^{-1}.

Another effective strategy to enhance SO_2 absorption and cycles performance was reported by Ilich A. Ibarra.[40] MIL-101(Cr) was redesigned with fluorine to promote the ability of SO_2 capture, named as MIL-101(Cr)-4F(1%). With the doping of

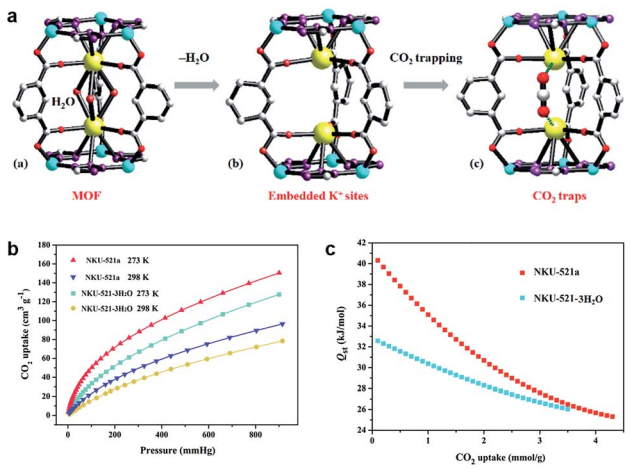

Fig. 2 (a) The structure of NKU-521, NKU-521a, and NKU-521a·CO_2 (according to the molecular simulation), (b) the CO_2 adsorption isotherms, (c) Q_{st} toward CO_2 for NKU-521-3H_2O and NKU-521a at 273 K and 298 K.[39] Reproduced from ref. 39 with permission, copyright John Wiley and Sons, 2019.

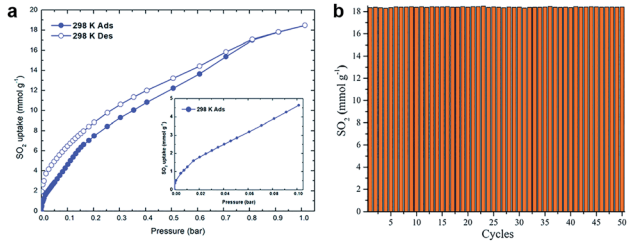

Fig. 3 (a) The SO_2 adsorption–desorption isotherm of MIL-101(Cr)-4F(1%), illustration: adsorption isotherm enlarged from 0.0–0.1 bar. (b) Adsorption–desorption cycles for 101(Cr)-4F(1%) at 298 K and 1 bar.[40] Reproduced from ref. 40 with permission, copyright The Royal Society of Chemistry, 2020.

fluorine, the acidity of open Cr(III) sites was significantly enhanced. Compared with MIL-101(Cr), MIL-101(Cr)-4F(1%) shows effective exaltation in SO_2 capture (18.4 mmol g^{-1}, 298 K, 1 bar), which attributed is to the difference of the attracting electron. At the same time, MIL-101(Cr)-4F(1%) also exhibited the adsorption–desorption stability of SO_2 (about 18.44 mmol g^{-1}, during 50 cycles), which ensures the development of adsorbents with high stability and long cycle life (Fig. 3).

There exist large sources of NH_3 in industry and daily life such as machines, the excrement of animals, and production in industry.[41] In order to integrate the adsorption capacity and cycle stability of the adsorbents, especially for corrosive gases. Taking into account the production cost and cycle stability, Li *et al.* focused on the M(BDC) (M = Cu, Zn, Cd) with structural

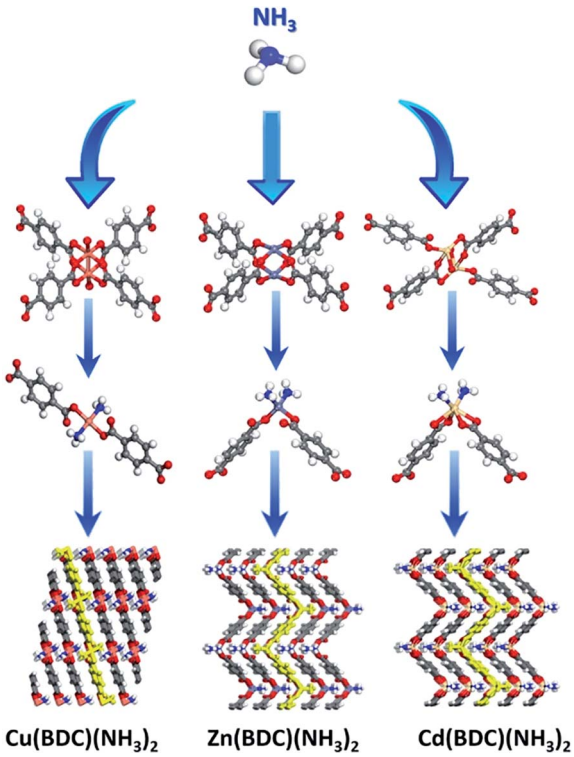

Fig. 4 The transform of M(BDC) (M = Cu, Zn, Cd).[42] Reproduced from ref. 42 with permission, copyright American Chemical Society, 2020.

transformation characteristics to explore a recyclable MOFs-based adsorbent.[42] While NH_3 touches with M(BDC) (M = Cu, Zn, Cd), the coordination model of the ligands will be transformed by the exchange of NH_3 and BDC ligands situated in the opposite position, leading to straight-chain (Cu(BDC)) or folded-chain (Zn(BDC) and Cd(BDC)) (Fig. 4). After transforming, the adsorption capacities of Cu(BDC), Zn(BDC), and Cd(BDC) are improved to 17.2, 14.1, and 7.4 mmol g^{-1}, respectively, realizing the removal of NH_3 even in air with a low concentration. Meaningfully, the transformation is proven to be completely reversible *via* extra activity at 250 °C for 80 minutes, which indicates the potential for recyclable industry application. Besides, Li's group also explored the enlarged preparation of Cu(BDC) and focused on the stability of the adsorbents, laying the groundwork for industrial-scale adsorbent production.[43]

2.2 Energy gas adsorption

With the consumption of traditional energy, such as petroleum, coal, and oil shale, people have begun to develop new clear energy sources such as hydrogen and methane to relieve the crisis caused by traditional energy.[44] However, current main gas storage and transportation methods are represented by pressurized liquefaction. Usually, it requires high pressure (up to 35–70 MPa at room temperature),[45] which compels the exploration of new measures to replace traditional physical storage.

At present, in order to enhance the banding density, many strategies usually focus on the design of the metal centers, such as open metal sites,[46] coordinatively unsaturated sites,[47] and open coordination sites.[48] Based on this, Long and co-workers reported $V_2Cl_{2.8}$(btdd), which exposes the V(II) sites to bond with weak π-acids, thus increasing the opportunities of H_2 capture.[18] Interestingly, this is the first material that exhibits binding enthalpy range between −15 kJ mol^{-1} and −25 kJ mol^{-1} (about −21 kJ mol^{-1}), and V(III) d_π and H_2 σ* orbital promote bond formation. Apart from improving the density and activity between gaseous substrates and effective metal sites; effective enclosed cages are also applied with gas capture. A typical example about MFM-132 ($[Cu_3(BTAT)(H_2O)_3]\cdot 9DMF$) was reported by Schröder and co-workers.[49] Desolvated MFM-132a functionalized by aromatic anthracene indicates that anthracene modification does not reduce the BET (reaching 2466 m^2 g^{-1}) or hinder the confirmation of porosity (pore volume = cm^3 g^{-1}); instead, it promotes the process of packing H_2 into the cages. It has been verified that the binding sites are composed of triangular $(Cu_2)_3$(isophthalate)$_3$ and three anthracene panels, forming the closed pockets of 6 Å. Under the same condition, MFM-132a realized the highest density of adsorbed H_2 within the pore, reaching 52 g L^{-1} at 60 bar and 77 K. In the long run, Schröder's works exploit a new direction for gas adsorption by aromatic connection units.

As the simplest hydrocarbon compound, CH_4 is considered as a clean energy as it does not produce any harmful gas, only CO_2 and H_2O. In addition, as the main component of natural gas (NG), developing the methods of efficient CH_4 storage is one of the keys to boost the application of NG.[50] At present, there are two main methods improving the NG volumetric energy density: Liquefied Natural Gas (LNG) and Compress Natural Gas (CNG). However, neither method is economical or convenient, especially in daily life. In this background, using MOFs adsorbent

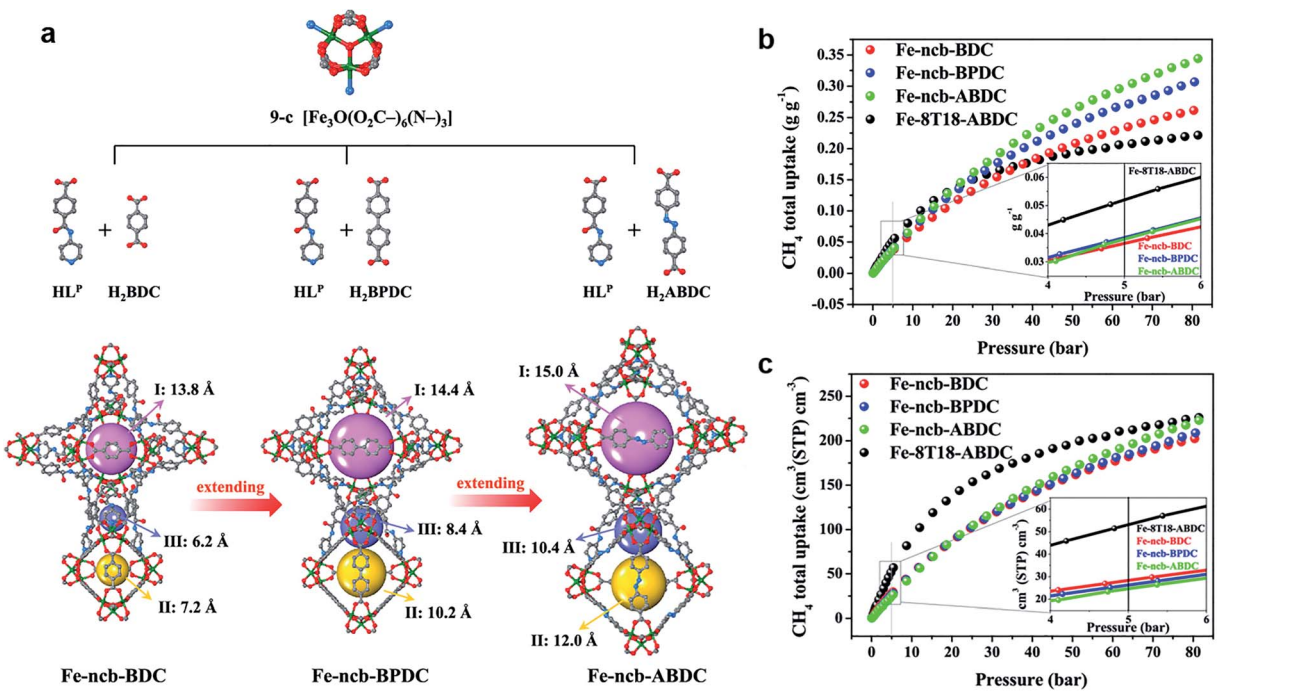

Fig. 5 (a) The constructions of Fe-ncb-MOFs. (b) The CH_4 gravimetric adsorption isotherms at 298 K. (c) Volumetric adsorption isotherms at 298 K.[51] Reproduced from ref. 51 with permission, copyright The American Chemical Society, 2021.

for gas storage is getting more and more attention. Similar to H_2 adsorption discussed above, a similar strategy is applied to CH_4 storage. As a comparison to the isoreticular structure, the linkers were extended from BDC to BPDC and ABDC. Three high-connected MOFs, including Fe-ncb-BDC ($[Fe_3O(L^P)_3(BDC)_{1.5}]\cdot x(solv)$), Fe-ncb-BPDC ($[Fe_3O(L^P)_3(BPDC)_{1.5}]\cdot x(solv)$), and Fe-ncb-ABDC ($[Fe_3O(L^P)_3(ABDC)_{1.5}]\cdot x(solv)$) were accurately synthesized.[51] Also, they exhibited increasing tendency of adsorption capacity with increasing ligand length to boost CH_4 storage effectively. Thus, Fe-ncb-ABDC exhibited the best performance due to the collaboration of confined hierarchical pores and open metal sites (Fig. 5). This is a rare example of CH_4 gravimetric and volumetric storage (reaching 0.302/0.37 g g^{-1}, 196/240 $cm_{(STP)}^3$ cm^{-3}, and 298/273 K, respectively) by blend high-connected MOFs, unlike the common low-connected MOFs. There is no doubt that the gravimetric working capacity at 65 bar of Fe-ncb-ABDC exhibits an obvious advantage compared with some benchmark works, such as HUKST-1, MAF-38, USTA-76, NJU-bai43, PCN-14, and MOF-905 (about 0.154, 0.176, 0.201, 0.221, 0.135, and 0.241 g g^{-1}, respectively).[52–58] Thus, the high-connected and mixed-linker strategy has proved to improve the CH_4 adsorption capacities.

In total, the design strategies taken in the above work are obviously diverse. Introducing unsaturated alkali-metal sites to NKU-521a is an effective way to enhance the binding stability between the host and the guest. MIL-101(Cr) and MFM-132a realize the functionalization of the framework environment by introducing functional groups. Focusing on the connected condition, high-connected mixed-linker Fe-ncb-MOFs result in the collaboration of confined hierarchical pores, further improving the performance for gas adsorption. For M(BDC), the spontaneous reversible transition after adsorption brings a new perspective to the study.

3. Gas separation

The mixed state is widespread and most gases exist as mixtures; thus, gas separation is still a significant process for the industry. However, there exist great challenges for precisely separating similar gas molecules, especially multi-components mixtures with slight differences.[59] Generally, cryogenic distillation, liquid adsorbent, and other traditional separation methods require high energy consumption, which greatly increases the industry costs. In contrast, adsorption is a relatively energy-saving and environment-friendly technology, and pressure swing adsorption and temperature swing adsorption are the main technologies for the industrial use of adsorbents. As new porous materials, MOFs have great advantages in gas separation. From the perspective of kinetics or others, many effective strategies, such as microporous engineering,[60] size screening,[61] and post-synthesis modification,[62] are accurately implemented to promote gas separation application. The precise design for MOFs allows that it can play a specific role for different separations by the diverse and designable construction at the molecular scale.

3.1 Alkynes/alkenes separation

The separation of alkyne and alkene mixtures is a challenging process. As shown in Table 1, there are many similarities (*e.g.*, close dynamic size, physical performances, and chemical performances), which bring out serious problems in the industry. In order to improve the separation efficiency (especially for separating the trace impurities) and relieve the pressure of the energy, environment, and the chemical industry, MOFs have received more and more attention as a typical adsorbent for separating C_2H_2/C_2H_4 and C_3H_4/C_3H_6.[63,64]

As we all know, when steam cracking C_2H_4 to obtain C_2H_6, C_2H_2 is generated as a by-product during this process.[65] It is universally known that C_2H_4 is mixed with small amount of C_2H_2. However, the presence of C_2H_2 is considered unfriendly due to its explosive properties and poisoning of Ziegler Natta catalysts during polymerization, which is not conducive for the economic industrial production. Thus, a typical truth is to find effective measures for separating the C_2H_2/C_2H_4 mixture securely. Based on it, Zhou and co-workers obtained NbU-1 ($(NH_4)\{Cu_3^{II}\cdot[Cu^{II}Cu_6^{I}(OH)_6(Ad)_6]_2\}\cdot(H_2O)_{10}$) to separate C_2H_2 and C_2H_4 by accessible and inexpensive materials.[66] In this work, NbU-1 showed the obvious separation of C_2H_2/C_2H_4 with the proportion of both 50 : 50 and 1 : 99 mixtures (Fig. 6). Importantly, C_2H_4 purity reaches 99.997% after separating, and the detection limit is lower than 0.003%, which is especially significant for the practical chemical industry application. It is worth noting that the excellent separation performance is contributed by the synergy of the open metal sites from heptanuclear metal cluster and the Lewis adsorption sites from the trigonal channel. Compared with the traditional separation

Table 1 The gas physical parameter

Gas	Acetylene	Ethylene	Ethane	Propyne	Propylene	Propane	Krypton	Xenon
Chemical formula	C_2H_2	C_2H_4	C_2H_6	C_3H_4	C_3H_6	C_3H_8	Kr	Xe
Model							—	—
Molecular weight	26.04	28.06	30.07	40.06	42.08	44.10	83.79	121.29
Dynamic size	3.3 Å	4.2 Å	4.4 Å	4.2 Å	4.7 Å	5.1 Å	3.7 Å	4.1 Å
Melting point	189.1 K	103.9 K	89.9 K	170.45 K	87.8 K	85.4 K	116 K	161 K
Boiling point	189.3 K	169.4 K	184.6 K	249.85 K	225.45 K	231.1 K	120 K	165 K

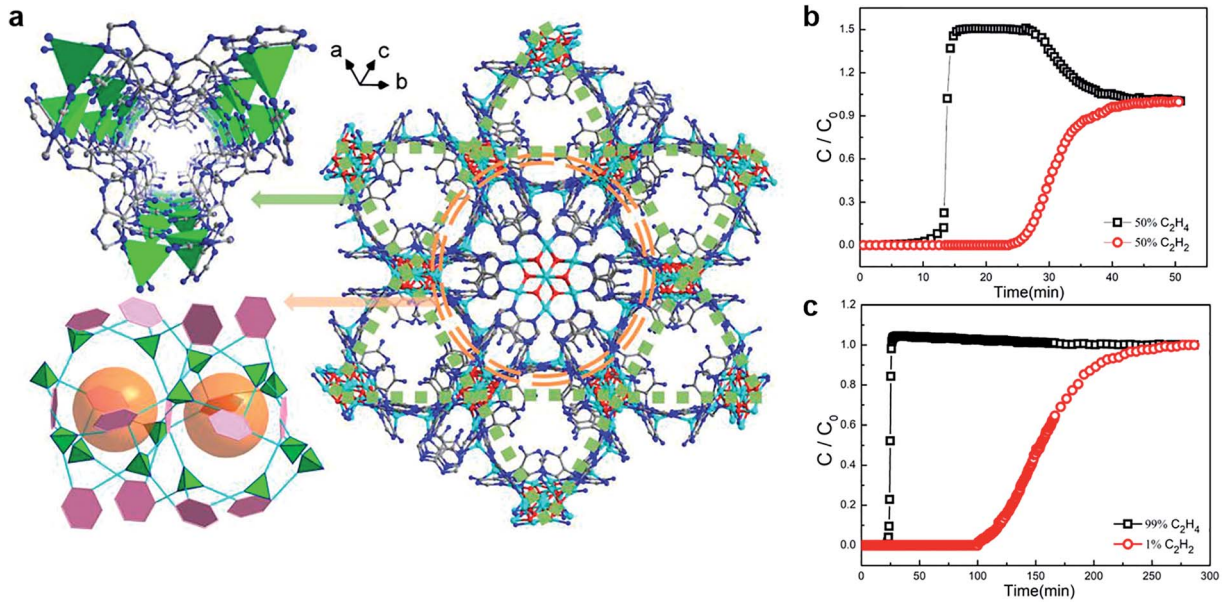

Fig. 6 (a) The channel and cavities in the 3D structure of NbU-1. (b) and (c) Breakthrough experiment for the mixture of C_2H_2 and C_2H_4 (50 : 50, 1 : 99, respectively).[66] Reproduced from ref. 66 with permission, copyright The American Chemical Society, 2019.

principle, NbU-1 brings into play the function of double Cu(I) sites where it supplies a rich electrical area for the guest molecules to combine into the frameworks. This ideal model exhibits potential in the precise design of MOFs, which broadens the application prospects in chemical separation.

In addition, the channel size of the MOFs is considered as one of the key factors for separating guest molecules. Except for the functional sites, regulating the pore size by the multi-level ligands length is one of the significantly visual ways to select the molecules. Some specific 3D frameworks are considered to be composed of 2D layers and supporting pillar ligand (*e.g.*, pyrazine, bipyridine, and other double connected linker). Some researchers are committed to designing the pore size according to the layer-pillar strategy, *i.e.*, adjusting the layer connector or pillar size. Yang *et al.* reported a series of MOFs termed as CPL-1 ($[Cu_2(pzdc)_2(pyz)\cdot 2H_2O]_n$), CPL-2 ($[Cu_2(pzdc)_2(bpy)\cdot 4H_2O]_n$), and CPL-5 ($[Cu_2(pzdc)_2(bpe)\cdot 5H_2O]_n$) by introducing pillared ligands (pyz, bpy, and bpe, respectively) as pillars.[67] As shown in Fig. 7, with the assistance of different pillar ligands, 4, 9, and 11 Å pores were constructed based on isoreticular chemistry. Since the suitable pores hinder the C_2H_4 into the skeleton, CPL-1 exhibits the best separation, which is an excellent case of a typical custom channel on MOFs.

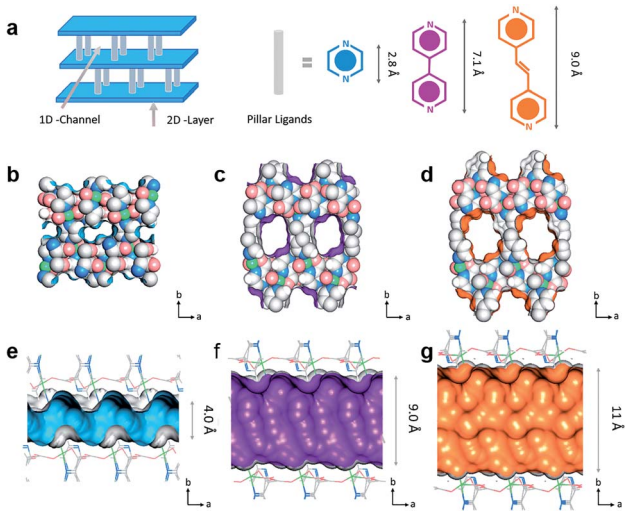

Fig. 7 (a) The crystal structure of $[Cu_2(pzdc)_2L]$. The pore constructed by three ligands of (b) and (e) CPL-1, (c) and (f) CPL-2, (d) and (g) CPL-5.[67] Reproduced from ref. 67 with permission, copyright The American Chemical Society, 2019.

Combining the two strategies of the metal sites and layer-pillar design, Qian *et al.* reported that Hofmann-type MOFs (ZJU-74a, $[Co(pyz)[Ni(CN)_4]]$ exhibited excellent C_2H_2/C_2H_4 separation performance, which is attributed to the ultra-strong C_2H_2 binding force from the $[Ni(CN)_4]^{2-}$ units and open metal sites in the sandwich-like structure.[68] As shown in Fig. 8, the breakthrough of C_2H_2 was observed at 140 min, and the C_2H_4 purity reached 99.9995% after separation. Qian's work offers a new direction to separate high purity C_2H_4 from the mixture of C_2H_4/C_2H_2 by capturing C_2H_2 precisely. On the one hand, compared with C_2H_4 adsorption to achieve separation, removing C_2H_2 is more practical and straightforward for industry application. On the other hand, this is a meaningful development to explore novel thinking under the guidance of precision design strategy.

Similarly, the mixed state of C_3H_4 and C_3H_6 is also ubiquitous and challenging for the chemical industry. Designing active metal sites is considered as an efficacious strategy for improving the effect of gas separation.[65] Yang *et al.* introduced two adsorption sites into GeFSIX-dps-M (M = Zn and Cu), and the metal in GeFSIX-dps-Zn was replaced completely to obtain

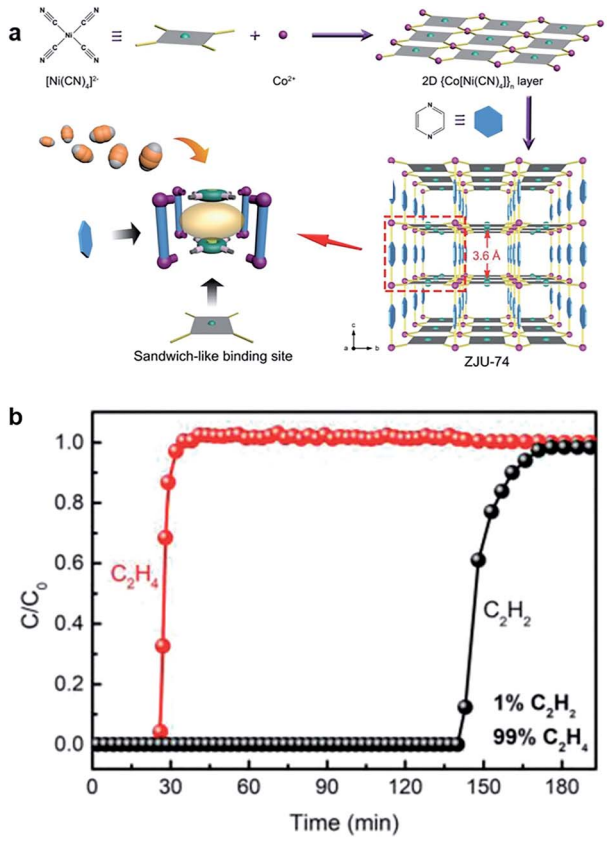

Fig. 8 (a) The construction process of ZJU-74a, 3D framework, and sandwich-like binding sites. (b) Experimental column breakthrough curves for a 1/99 C_2H_2/C_2H_4 mixture at 298 K and 1 bar.[68] Reproduced from ref. 68 with permission, copyright John Wiley and Sons, 2020.

GeFSIX-dps-Cu ($[Cu(dps)_2(GeF_6)]$).[69] Surprisingly, due to effective H-bonding sites in the pore and interlayer space, the tiny connector and fine-tuning in the layer state enhanced the selectivity of C_3H_4/C_3H_6 significantly. In this way, alkyne was easier to be allowed into the pore space than the alkene to meet the demands of molecular screening, which was confirmed by both the crystal structure and calculation of C_2H_4-combined GeFSIX-dps-Cu. In GeFSIX-dps-Cu, site II was combined with C_3H_4, and it is worth mentioning that the guest-binding behaviour can be observed by the intuitive crystal structure (Fig. 9) even after adsorption, which were also verified by density functional theory (DFT-D).

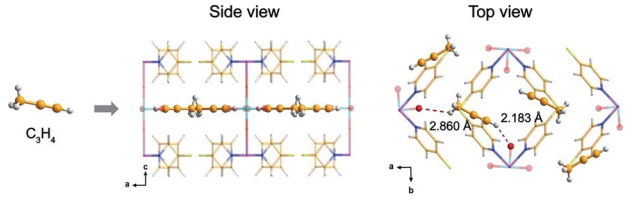

Fig. 9 Schematic diagram of GeFSIX-dps-Cu after adsorbing C_3H_4.[69] Reproduced from ref. 69 with permission, copyright John Wiley and Sons, 2020.

3.2 Alkanes/alkenes separation

As one of the most significant raw materials, C_2H_4 and C_3H_6 are the key industry chemicals in plastics manufacturing, and they are usually produced by cracking naphtha.[70] Generally, "polymer-grade" is the basic requirement for the manufacture of plastics,[71] which means that high-purity alkanes need to be obtained economically. However, some by-products such as alkanes are produced during the process of cracking. Therefore, it is really essential to develop effective measures for separating alkanes and alkenes.

C_2H_4 is considered as the core of the petroleum and chemical industry, and the productivity of C_2H_4 is one of the criteria for judging the industrial level. Adjusting the size and functionalizing the pore environment are the most direct ways to enhance the gas separation performance. Generally, due to the interaction between C_2H_6 molecules and MOFs skeleton not being strong, most researchers focused on enhancing the interaction between C_2H_6 and frameworks to get high purity C_2H_4 in one-step.[72] Qian *et al.* designed the pore environment by introducing the nonpolar naphthalene and anthracene to obtain ZJU-120 ($Ni(ndc)(ted)_{0.5}$) and ZJU-121 ($Ni(adc)(ted)_{0.5}$)[60] (Fig. 10). In this way, the pore size was limited to 4.4 Å and 3.7 Å for ZJU-120 and ZJU-121, respectively, which is caused by both steric hindrance inside the pore and the significant increase in the density of the nonpolar aromatic system. Compared with $Ni(bpc)(ted)_{0.5}$ and ZJU-121a, due to the suitable pore size, ZJU-120a can effectively adsorb C_2H_6 (96 $cm^3\ g^{-1}$ at 296 K, 0.5 bar) and exhibit excellent C_2H_6/C_2H_4 separation behavior (2.74, IAST selectivity). Controlling the microporous size and polarity by enhancing the C_2H_6 interaction effectively realized the separation of C_2H_6/C_2H_4.

Besides, there are many persuasive examples of functional modification. Ma *et al.* obtained $Ni(TMBDC)(DABCO)_{0.5}$ with high C_2H_6 uptake (up to 2.21 mmol g^{-1}, 0.0625 bar) by controlling the ligand methyl-functionalization, supplying potential advantages for separation.[73] Through substituent engineering, He *et al.* contrasted a series of MOFs modified with different branch chain, including ZJNU-21 ($[Cu(L_2)]\cdot DMF\cdot CH_3OH$), ZJNU-22 ($[Cu(L_3)]\cdot 0.5DMF\cdot CH_3OH$), ZJNU-23 ($[Cu(L_4)]\cdot DMF$), and the maternal structure was named NJU-Bai7. The result also revealed that methyl is a significant functional group to elevate the separation performance.[74] Similarly, with methylation, Noro *et al.* observed the apparent confinement effect to limit the guest into the channel.[75] These are representative samples by functionalization to elevate the separation efficiency.

Furthermore, constructing MOFs with excellent separation performance requires finding out the relationships among the structure modules and performing precise design from multiple angles. In 2020, Krishna *et al.*[76] designed 9 kinds of contrastive structure to research the structure–performance relations from three aspects including ligands (*e.g.*, H_2BDC and H_2DMBDC), pore-partitioning linker (*e.g.*, TPT, TPBz, and TPPy) and metal cluster (*e.g.*, Co_2V, Co_2Ti, Mg_2V, and Mg_2Ti) (Fig. 11). These contrasts of the material family indicated that BDC plays a leading role in adsorption, and TPT has a main effect on $C_2H_6/$

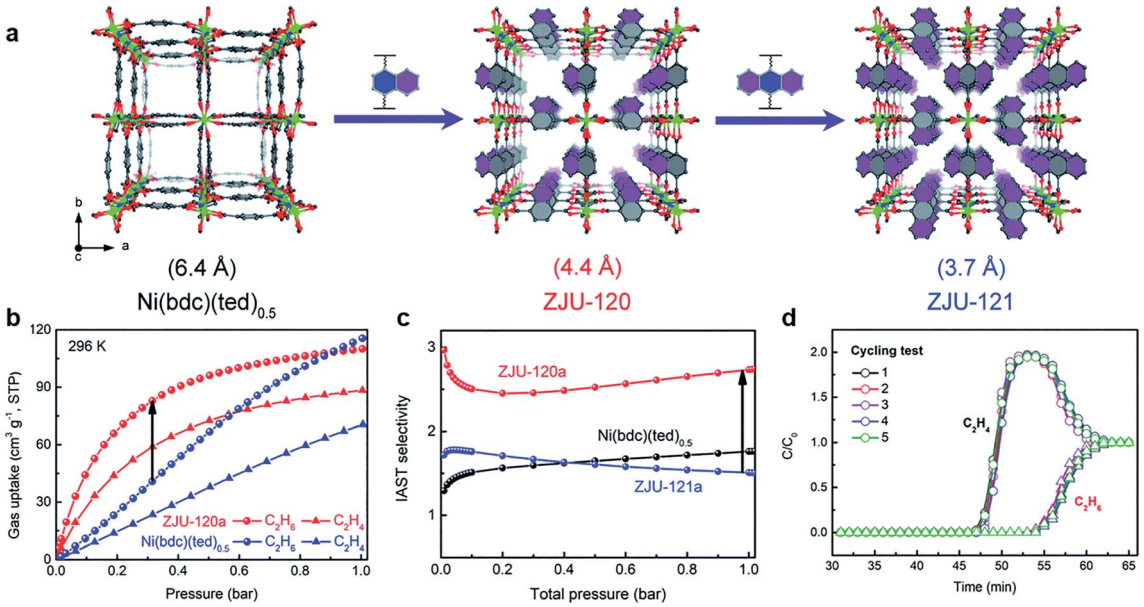

Fig. 10 (a) Structure of Ni(bdc)(ted)0.5, ZJU-120, and ZJU-121 constructed by introducing different aromatic rings. (b) Gas adsorption isotherms of ZJU-120a and Ni(bdc)(ted)$_{0.5}$ for C_2H_6 and C_2H_4 (196 K). (c) IAST selectivity for C_2H_6/C_2H_4 (50 : 50, 296 K). (d) Cycling test of ZJU-120 for the C_2H_6/C_2H_4 (50 : 50, 298 K, 1 bar, 1.25 mL min^{-1}).[60] Reproduced from ref. 60 with permission, copyright The Royal Society of Chemistry, 2020.

C_2H_4 separation. For metal center, the highest C_2H_6 uptake (up to 166.8 cm^3 g^{-1}) was achieved by Mg_2V-bdc-tpt (Mg_2-V(OH)(bdc)$_3$tpt); the most excellent C_2H_2/C_2H_4 separation performance (with 50/50) was obtained by Co_2V-bdc-tpt (Co_2-V(OH)(bdc)$_3$tpt), and both them could separate C_2H_4 from the mixture with high purity (up to 99.95%). The influence of three compositions on C_2H_6/C_2H_4 separation were systematically discussed in order to reveal the relationships between the separation and the module. The crystal engineering of the linker precisely designs a microporous environment as an achievable method for absorbing and separating instructively.

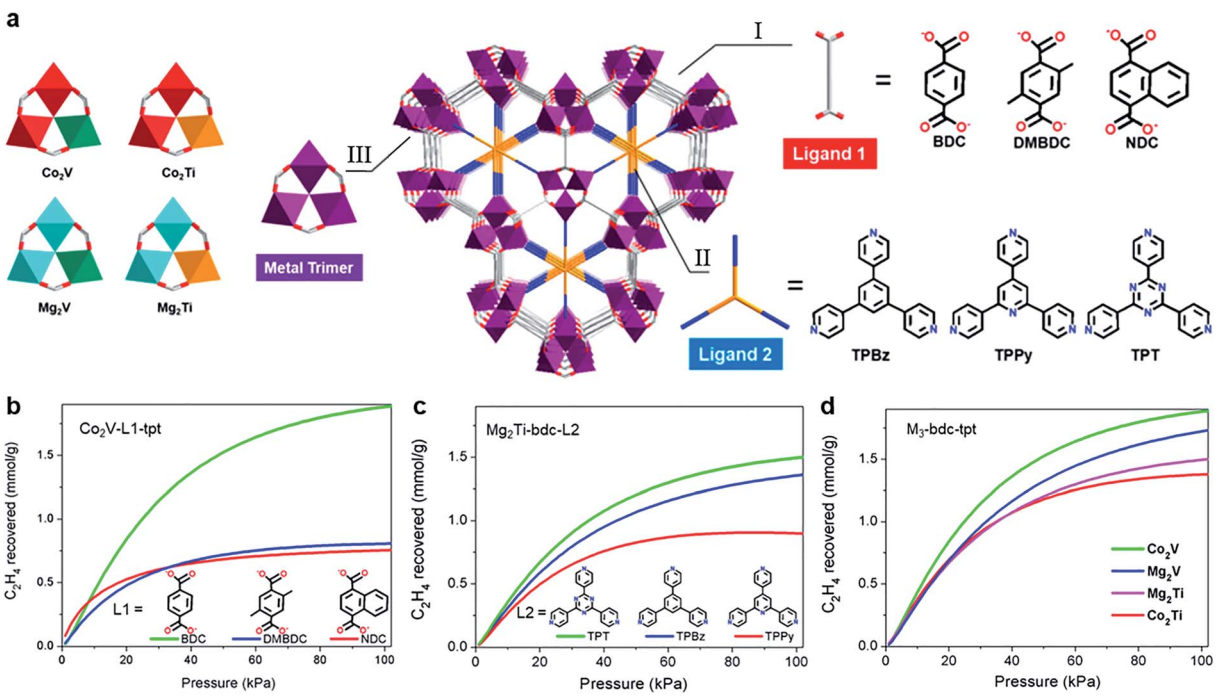

Fig. 11 (a) The frameworks composed by three kinds of ligand 1, three kinds of ligand 2, and four kinds of metal cluster. (b) Contradistinction of C_2H_6/C_2H_4 (50/50) separation potential of Co_2V-L1-tpt, (c) Mg_2Ti-bdc-L_2, and (d) M_3-bdc-tpt.[76] Reproduced from ref. 76 with permission, copyright The American Chemical Society, 2020.

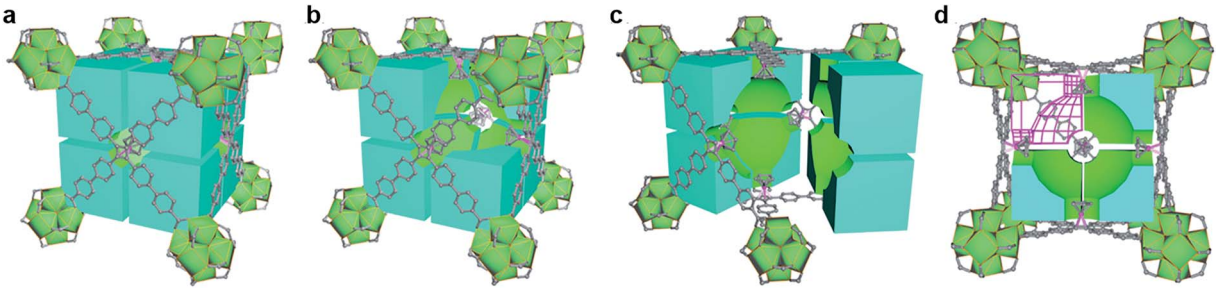

Fig. 12 Structural illustration of UPC-612 with cage filling. (a) Cubic cage filling of a basic unit in UPC-612; (b) space division of cubic cage; (c) internal space allocation of UPC-612 after partition; (d) cubic cage filling profile and a sphere like force surface.[77] Reproduced from ref. 77 with permission, copyright John Wiley and Sons, 2021.

Functional modification based on open topological platform promotes the universality study of MOFs. Recently, based on the stable high-valance MOFs, our group reported new pore environment modification by introducing cyclopentadiene cobalt functional group to selectively enhance the interaction between the frameworks and the guest.[77] In two typical Zr-MOFs

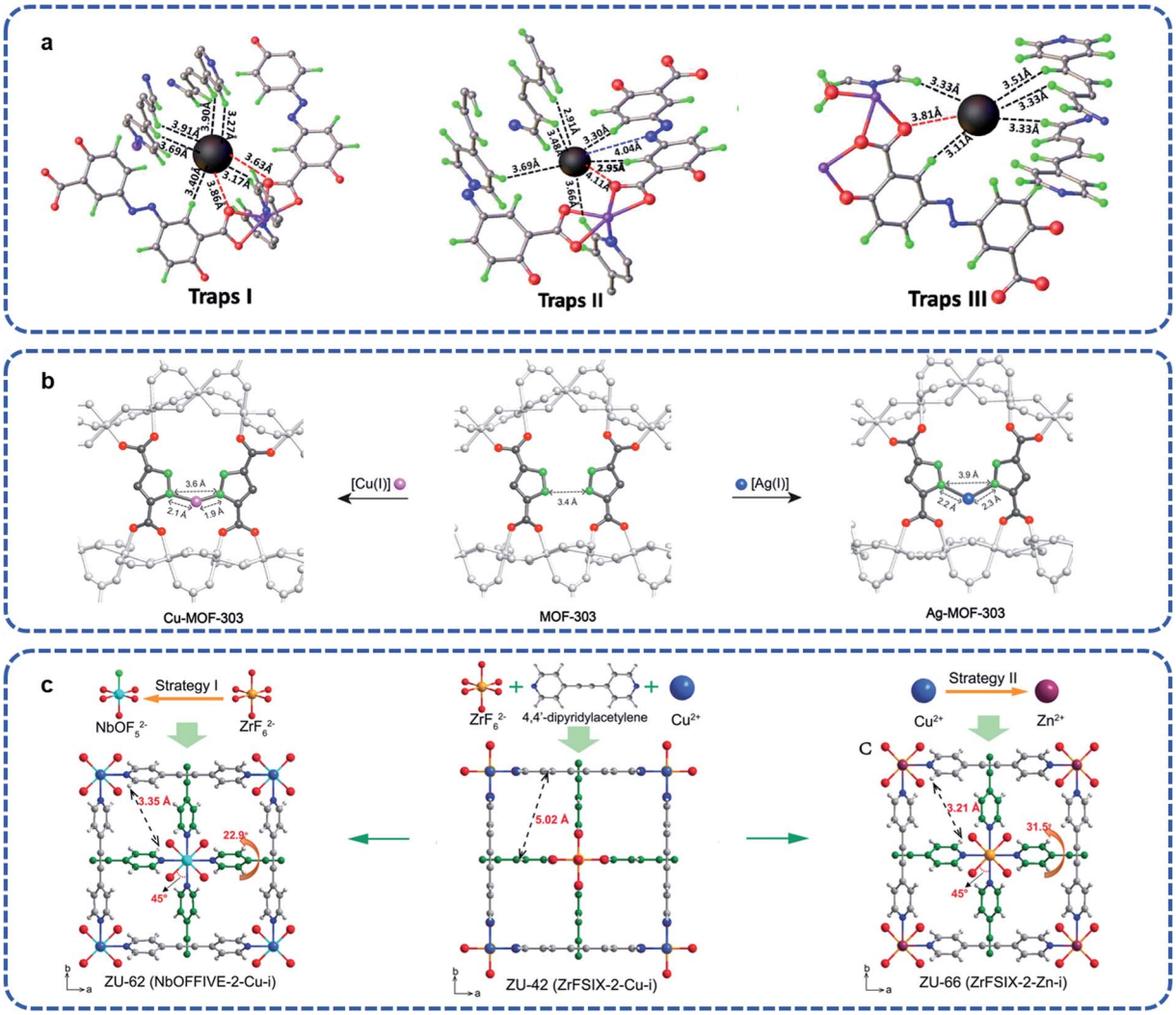

Fig. 13 (a) Three adsorption traps in ECUT-60.[82] Reproduced from ref. 82 with permission, copyright Elsevier, 2021. (b) The chelated structure of Cu-MOF-303 and Ag-MOF-303 derived from MOF-303.[62] Reproduced from ref. 62 with permission, copyright John Wiley and Sons, 2020. (c) The interpenetrated networks of ZU-62, ZU-42, and ZU-66 (viewed along the *c*-axis).[84] Reproduced from ref. 84 with permission, copyright John Wiley and Sons, 2020.

(UPC-612 and UPC-613), isomorphic ligands were used to construct different size cage in which differential guest binding behavior can be precisely achieved. Thus, both UPC-612 and UPC-613 could purify the C_2H_4/C_2H_6 or C_2H_4/C_2H_2 mixture to obtain polymer grade C_2H_4. It is worth mentioning that even under 10% content of C_2H_2 or C_2H_6, UPC-612 remains the highest separation potential. Furthermore, as a more general state, the ternary mixture of $C_2H_6/C_2H_4/C_2H_2$ could be separated, abstracting C_2H_4 in one step. As the first work in one-step C_2H_4 purification from large proportion ternary mixtures, the spherical force surface formed in the cage modified by cyclopentadiene cobalt serves as strong evidence for precisely controlling the pore environment for one-step purification (Fig. 12).

3.3 Noble gas separation

As the physically and chemically stability gases, noble gases, such as He, Ne, Ar, Kr, and Xe, are widely applied to the medical, electronic component, lighting, and space industry.[78] There exist mixtures of noble gases in the off-gases such as used nuclear fuel (UNF) and it is an essential industrial process to separate each component.[79–81] However, compared with light hydrocarbon separation, it is a well-known challenge to separate single noble gases component from the mixed state economically and effectively due to the similar physical and chemical properties. Besides, since the actual application environments of noble gas separation is more complex, on the basis of satisfying the working capacity, more research should focus on the material tolerance to complex environments, such as humidity, corrosive, and acid-base environments.

Introducing effective site strategy is one of the direct approaches to elevate guest combination behavior. In order to obtain high purity Xe, Luo *et al.* explored stable MOFs defined ECUT-60 (Co_2(bpe)(OLZ^{4-})) as a potential candidate separating Xe from the off-gases.[82] The advantages of both capture load and separation come from the direct restriction from Xe by the van der Waals force. There are three sites that supply the higher binding energy for Xe (-46.05 kJ mol^{-1}, -40.93 kJ mol^{-1}, and -45.53 kJ mol^{-1}, respectively), which indicates the priority opportunity for Xe adsorption (Fig. 13a). Similarly, dual sites of NKMOF-1-Ni reported by Zhao *et al.* guarantee the separation not only in the mixture of Xe/Kr but also Xe/Ar and Xe/N_2, which was investigated by the Q_{st} (about 34.2 kJ mol^{-1}) and the calculation of the Xe potential field.[83]

Based on the MOF-303 ([Al(OH)($C_5H_2O_4N_2$)]), Yaghi *et al.* reported that the chelation of Cu^I or Ag^I on the atom scale can

Table 2 The gas separation data of the MOFs reported in recent year

MOFs	Metal	Pore size (Å)	Mixed gas	Q_{st}[a] (kJ mol^{-1})	Selectivity[b]	Uptake[d]	Temp. (K)	Ref.
NbU-1	Cu	4	C_2H_2/C_2H_4	38.3 (C_2H_2), 37.9 (C_2H_4)	12.1, C_2H_2/C_2H_4 = 50 : 50 5.9, C_2H_2/C_2H_4 = 50 : 50	81.5[e] (C_2H_2) 53.1[e] (C_2H_2)	273 298	66
CPL-1	Na	4	C_2H_2/C_2H_4	40.2 (C_2H_2), 36.8 (C_2H_4)	26.75, C_2H_2/C_2H_4 = 1 : 99	2.07[f] (C_2H_2), 0.31[f] (C_2H_4)	298	67
CPL-2	Na	9	C_2H_2/C_2H_4	30.8 (C_2H_2), 20.3 (C_2H_4)	12, C_2H_2/C_2H_4 = 1 : 99	3.13[f] (C_2H_2), 1.86[f] (C_2H_4)	298	67
CPL-5	Na	11	C_2H_2/C_2H_4	31.3 (C_2H_2), 19.1 (C_2H_4)	5.99, C_2H_2/C_2H_4 = 1 : 99	3.01[f] (C_2H_2), 1.84[f] (C_2H_4)	298	67
ZJU-74a	Co	3.9	C_2H_2/C_2H_4	45–65 (C_2H_2)[c]	24.2, C_2H_2/C_2H_4 = 50 : 50	49[e] (C_2H_2)	296	68
GeFSIX-dps-Cu	Cu	—	C_2H_2/C_2H_4	—	40.1, C_2H_2/C_2H_4 = 50 : 50	4.28[f] (C_2H_2), 0.16[f] (C_2H_4)	298	69
		—	C_3H_4/C_3H_6	—	36.45, C_3H_4/C_3H_6 = 50 : 50	3.73[f] (C_3H_4), 0.08[f] (C_3H_6)	298	
ZJU-120a	Ni	4.4	C_2H_6/C_2H_4	27.6 (C_2H_6)	2.74, C_2H_6/C_2H_4 = 50 : 50	4.91[f] (C_2H_6), 3.93[f] (C_2H_4)	296	60
ZJU-121a	Ni	3.7	C_2H_6/C_2H_4	47.1 (C_2H_6), 43.0 (C_2H_4)	1.51, C_2H_6/C_2H_4 = 50 : 50	3.1[f] (C_2H_6), 3.19[f] (C_2H_4)	296	60
CPM-733	Co, V	7.3	C_2H_6/C_2H_4	23.4 (C_2H_6), 22.5 (C_2H_4)	1.75, C_2H_6/C_2H_4 = 50 : 50	159.6[e] (C_2H_6), 142.7[e] (C_2H_4)	298	76
ZJNU-21	Cu	—	C_2H_6/C_2H_4	37.36 (C_2H_6), 33.87 (C_2H_4)	1.65, C_2H_6/C_2H_4 = 50 : 50	72.7[e] (C_2H_6), 71.4[e] (C_2H_4)	298	74
ZJNU-22	Cu	—	C_2H_6/C_2H_4	37.32 (C_2H_6), 35.47 (C_2H_4)	1.34, C_2H_6/C_2H_4 = 50 : 50	65.6[e] (C_2H_6), 64.2[e] (C_2H_4)	298	74
ZJNU-23	Cu	—	C_2H_6/C_2H_4	35.42 (C_2H_6), 35.11 (C_2H_4)	1.23, C_2H_6/C_2H_4 = 50 : 50	66.4[e] (C_2H_6), 65.6[e] (C_2H_4)	298	74
ECUT-60	Co	4.5	Xe/Kr	30 (Xe), 22.6 (Kr)	11.36, Xe/Kr = 20 : 80	4.3[f] (Xe), 1.45[f] (Kr)	298	82
NKMOF-1-Ni	Ni	5.36	Xe/Kr	34.2 (Xe), 33.1 (Kr)	5.2, Xe/Kr = 20 : 80	2.47[f] (Xe), 1.86[f] (Kr)	273	83
			Xe/Ar	34.2 (Xe), 26.1 (Ar)	41.3, Xe/Ar = 1 : 99	2.47[f] (Xe), 0.84[f] (Ar)	273	
Ag-MOF-303	Ag, Al	5.2	Xe/Kr	28.2 (Xe)	10.4, Xe/Kr = 20 : 80	108[e] (Xe)	298	62
Cu-MOF-303	Cu, Al	5.5	Xe/Kr	24.4 (Xe)	8.2, Xe/Kr = 20 : 80	91[e] (Xe)	298	62

[a] Q_{st} values at zero coverage. [b] Selectivity is calculated by IAST. [c] The highest Q_{st} values at various surface coverage. [d] Adsorption uptake obtained from single-component gas adsorption isotherms. [e] cm^3 g^{-1}, at 1 bar. [f] mmol g^{-1}, at 1 bar.

effectively control the pore size to match with Xe, and obtain the derived Cu-MOF-303 and Ag-MOF-303.[62] As shown in Fig. 13b, the ligands alternately distributed on both sides of the 1D chain-shaped SBU provide exposed sites for further chelation with metal ions, which reveals the strategy using additional binding sites to match the guest size, and allows the combination of ultrahigh selectivity and uptake. For Ag-MOF-303, it showed unexpected improvement in both Xe adsorption (up to 59 cm^{-3} cm^{-3} at 298 K) and Xe/Kr selectivity (about 10.4, v/v = 20/80). From this perspective, it increased to twice as much as that of the original material MOF-303.

In addition to designing the sites directly, the frameworks' self-properties can respond to guest touch. Yang *et al.* reported interpenetrated ZU-62 ($Cu(dpa)_2(NbOF_5)$) with accurate anion pillared pore environment.[84] Once the Xe guest gets in touch with the cavity, the size and shape can be adjusted by pillar and pyridine spinning to accommodate the Xe atoms, leading to the expansion of the pore size, which is completely different with Kr atoms. Due to the stronger polarity of the Xe atoms, a significant open pore state was caused by the interaction force between the skeleton and the guests. In total, the purification of Kr directly or the desorption of Xe after adsorption, both methods could obtain high capacity and purity (206 mL g^{-1}, >99.9%; 42 mL g^{-1}, >99.9%; respectively).

In total, by utilizing intuitive size sieving, CPL-1 and MOF-303 can effectively identify the size difference between guest molecules and achieve mixture separation. By designing the binding sites, both NbU-1 and ZJU-74 can achieve efficient and selective adsorption. Modulating host–guest interactions can be achieved through functional group modification (such as ZJU-120a and UPC-612), metal nodes control (such as GeFSIX-dps-Cu), enhancing van der Waals force (such as ECUT-60) and flexible structure transform (such as ZU-62). Further, it is a more meaningful design idea to give full play to the above strategies to form a synergistic effect.

Table 3 Abbreviation for the compounds

Abbreviation	Compounds
H_3TZIA	5-(1*H*-Tetrazol-5-yl)isophthalic acid
BDC	1,4-Dicarboxybenzene
H_2btdd	Bis(1*H*-1,2,3-triazolo[4,5-*b*],[4′,5′-*i*])dibenzo[1,4]dioxin
H_6BTAT	5,5′,5″-(Benzene-1,3,5-triyltris(anthracene-10,9-diyl)) triisophthalic acid
BPDC	4,4′-Biphenyldicarboxylate
ABDC	Azobenzene-4,4′-dicarboxylate
L^P	4-(Pyridin-4-ylcarbamoyl)benzoate
Ad	Adenine
pyz	Pyrazine
bpy	4,4′-Bipyridine
bpe	*trans*-1,2-Di(4-pyridyl)-ethylene
pyz	Pyrazine
dps	4,4′-Dipyridylsulfide
H_2ndc	1,4-Naphthalenedicarboxylic acid
DABCO or ted[a]	1,4-Diazabicyclo[2.2.2]octane
H_2adc	9,10-Anthracenedicarboxylic acid
TMBDC	2,3,5,6-Tetramethylterephthalic acid
H_2L_2 (in ZJNU-21)	5-(5-Methylpyridin-3-yl)isophthalic acid
H_2L_3 (in ZJNU-22)	5-(5-Methoxypyridin-3-yl)isophthalic acid
H_2L_4 (in ZJNU-23)	5-(5-Chloropyridin-3-yl)isophthalic acid
H_2BDC	1,4-Benzenedicarboxylic acid
H_2NDC	1,4-Naphthalenedicarboxylic acid
H_2DMBDC	2,5-Dimethylterephthalic acid
TPT	2,4,6-Tri(4-pyridyl)-1,3,5-triazine
TPBz	2,4,6-Tri(4-pyridyl)benzene
TPPy	2,4,6-Tri(4-pyridyl)pyridine
bpe	1,2-Bis(4-pyridyl)ethylene
OLZ^{4-}	Olsalazine
dpa	4,4′-Dipyridylacetylene

[a] Different abbreviations for the same molecule.

4. Conclusion and outlook

Gas adsorption and separation are necessary scientific topics for industrial activities. The designable and controllable structure of the MOFs implies that further development is imperative. We reviewed recent representative researches of gas storage or removal, light hydrocarbon, and noble gas separation, and analyzed the inspirations and characteristics from ligands/metal nodes design, active combination sites construction, SBU modification, pore division, and other multiple perspectives, providing guidance for designing adsorption/separation-oriented MOFs.

At present, MOFs with excellent performance have been widely reported (Table 2). Specifically, pore environment and framework conformation are key to host–guest interactions; thus, how to further sensitively achieve molecules capturing by multi-level crystal engineering is still a key issue needed to be researched thoroughly. In addition, to practically optimize the potential application of the absorbent, the following aspects should be further considered.

(i) Taking into account the complex surroundings, stable adsorbent-like high-valence MOFs should receive further attention to adequately address the changeable condition, especially water/acid system, thermal stability, cycle-life, *etc.*

(ii) Explore environments-friendly synthetic methods, and reduce the organic solvents usage rate to meet the requirements of both clean and scale-up manufacture.

(iii) How to maximally reduce the production cost by exploring more inexpensive raw material and production process.

(iv) Research must also focus more on promoting the production scale, expanding to meet the industrial scenarios.

In conclusion, based on the irreplaceable development potential, more comprehensively precise design strategies will greatly promote the pace of MOFs materials as industrial adsorption/separation carriers (Table 3).

Author contributions

Chuanhai Jiang: data collection, validation, conceptualization, writing – original draft. Xiaokang Wang: data collection, visualization, validation. Yuguo Ouyang: data collection,

visualization, validation. Kebin Lu: data collection, visualization, validation. Weifeng Jiang: data collection, visualization, validation. Huakai Xu: data collection, visualization, validation. Xiaofei Wei: data collection, visualization, validation. Zhifei Wang: data collection, visualization, validation. Fangna Dai: supervision, visualization, writing & editing, project administration, funding acquisition. Daofeng Sun: supervision, project administration, funding acquisition.

Conflicts of interest

There are no conflicts to declare.

Acknowledgements

This work was supported by the Natural Science Foundation of Shandong Province (ZR2020KB010); the National Natural Science Foundation of China (21771191); and the Fundamental Research Funds for the Central Universities (19CX05001A).

Notes and references

1 S. L. James, *Chem. Soc. Rev.*, 2003, **32**, 276–288.
2 O. M. Yaghi, G. Li and H. Li, *Nature*, 1995, **378**, 703–706.
3 L. Jiao, J. Y. R. Seow, W. S. Skinner, Z. U. Wang and H. Jiang, *Mater. Today*, 2019, **27**, 43–68.
4 I. Stassen, N. Burtch, A. Talin, P. Falcaro, M. Allendorf and R. Ameloot, *Chem. Soc. Rev.*, 2017, **46**, 3185–3241.
5 G. L. Yang, X. L. Jiang, H. Xu and B. Zhao, *Small*, 2021, **17**, 2005327.
6 Z. Xiao, Y. Wang, B. Xu, S. Du, W. Fan, D. Cao, Y. Deng, L. Zhang, L. Wang and D. Sun, *Adv. Sci.*, 2020, **7**, 2000065.
7 Z. Q. Wang, H. Q. Luo, Y. L. Wang, M. Y. Xu, C. T. He and Q. Y. Liu, *Inorg. Chem.*, 2021, **60**, 10596–10602.
8 C. Wang, B. An and W. Lin, *ACS Catal.*, 2018, **9**, 130–146.
9 S. Mallakpour, E. Nikkhoo and C. M. Hussain, *Coord. Chem. Rev.*, 2022, **451**, 214262.
10 X. Zhang, H. Cui, R. B. Lin, R. Krishna, Z. Y. Zhang, T. Liu, B. Liang and B. Chen, *ACS Appl. Mater. Interfaces*, 2021, **13**, 22514–22520.
11 H. Cui, Y. Ye, T. Liu, Z. A. Alothman, O. Alduhaish, R. B. Lin and B. Chen, *Inorg. Chem.*, 2020, **59**, 17143–17148.
12 E. Chapman, S. Ullah, H. Wang, L. Feng, K. Wang, H. C. Zhou, J. Li, T. Thonhauser and K. Tan, *ACS Appl. Mater. Interfaces*, 2021, **13**, 43661–43667.
13 W. Fan, S. Yuan, W. Wang, L. Feng, X. Liu, X. Zhang, X. Wang, Z. Kang, F. Dai, D. Yuan, D. Sun and H. C. Zhou, *J. Am. Chem. Soc.*, 2020, **142**, 8728–8737.
14 R. Lin, S. Xiang, W. Zhou and B. Chen, *Chem*, 2020, **6**, 337–363.
15 Y. Jiang, T. Hu, L. Yu and Y. Ding, *Nanoscale Adv.*, 2021, **3**, 4079–4088.
16 C. Jiang, X. Wang, K. Lu, W. Jiang, H. Xu, X. Wei, Z. Wang, Y. Ouyang and F. Dai, *J. Solid State Chem.*, 2022, **307**, 122881.
17 D. Wu, P. Zhang, G. Yang, L. Hou, W. Zhang, Y. Han, P. Liu and Y. Wang, *Coord. Chem. Rev.*, 2021, **434**, 213709.
18 D. E. Jaramillo, H. Z. H. Jiang, H. A. Evans, R. Chakraborty, H. Furukawa, C. M. Brown, M. Head-Gordon and J. R. Long, *J. Am. Chem. Soc.*, 2021, **143**, 6248–6256.
19 T. Yoskamtorn, P. Zhao, X. P. Wu, K. Purchase, F. Orlandi, P. Manuel, J. Taylor, Y. Li, S. Day, L. Ye, C. C. Tang, Y. Zhao and S. C. E. Tsang, *J. Am. Chem. Soc.*, 2021, **143**, 3205–3218.
20 A. M. Wright, C. Sun and M. Dinca, *J. Am. Chem. Soc.*, 2021, **143**, 681–686.
21 J. Perego, C. X. Bezuidenhout, A. Pedrini, S. Bracco, M. Negroni, A. Comotti and P. Sozzani, *J. Mater. Chem. A*, 2020, **8**, 11406–11413.
22 T. D. Duong, S. A. Sapchenko, I. da Silva, H. G. W. Godfrey, Y. Cheng, L. L. Daemen, P. Manuel, M. D. Frogley, G. Cinque, A. J. Ramirez-Cuesta, S. Yang and M. Schröder, *Chem. Sci.*, 2020, **11**, 5339–5346.
23 P. Brandt, S. H. Xing, J. Liang, G. Kurt, A. Nuhnen, O. Weingart and C. Janiak, *ACS Appl. Mater. Interfaces*, 2021, **13**, 29137–29149.
24 P. Brandt, A. Nuhnen, M. Lange, J. Mollmer, O. Weingart and C. Janiak, *ACS Appl. Mater. Interfaces*, 2019, **11**, 17350–17358.
25 X. Zhao, Y. Wang, D. S. Li, X. Bu and P. Feng, *Adv. Mater.*, 2018, **30**, 1705189.
26 X. Y. Li, Z. J. Li, Y. Z. Li, L. Hou, Z. Zhu and Y. Y. Wang, *Inorg. Chem.*, 2018, **57**, 12417–12423.
27 X. Liu, W. Fan, M. Zhang, G. Li, H. Liu, D. Sun, L. Zhao, H. Zhu and W. Guo, *Mater. Chem. Front.*, 2018, **2**, 1146–1154.
28 E. Binaeian, Y. Li and D. Yuan, *Chem. Eng. J.*, 2021, **421**, 129655.
29 H. S. Papastathopoulou and W. L. Luyben, *Ind. Eng. Chem. Res.*, 1991, **30**, 705–713.
30 L. Li, R. Lin, X. Wang, W. Zhou, L. Jia, J. Li and B. Chen, *Chem. Eng. J.*, 2018, **354**, 977–982.
31 S. Yang, A. J. Ramirez-Cuesta, R. Newby, V. Garcia-Sakai, P. Manuel, S. K. Callear, S. I. Campbell, C. C. Tang and M. Schroder, *Nat. Chem.*, 2014, **7**, 121–129.
32 O. Karagiaridi, W. Bury, E. Tylianakis, A. A. Sarjeant, J. T. Hupp and O. K. Farha, *Chem. Mater.*, 2013, **25**, 3499–3503.
33 N. Huang, S. Yuan, H. Drake, X. Yang, J. Pang, J. Qin, J. Li, Y. Zhang, Q. Wang, D. Jiang and H. C. Zhou, *J. Am. Chem. Soc.*, 2017, **139**, 18590–18597.
34 W. Fan, X. Wang, X. Liu, B. Xu, X. Zhang, W. Wang, X. Wang, Y. Wang, F. Dai, D. Yuan and D. Sun, *ACS Sustainable Chem. Eng.*, 2018, **7**, 2134–2140.
35 Q. G. Zhai, X. Bu, X. Zhao, D. S. Li and P. Feng, *Acc. Chem. Res.*, 2017, **50**, 407–417.
36 H. Wang, D. Luo, E. Velasco, L. Yu and J. Li, *J. Mater. Chem. A*, 2021, **9**, 20874–20896.
37 M. Ding, R. W. Flaig, H. L. Jiang and O. M. Yaghi, *Chem. Soc. Rev.*, 2019, **48**, 2783–2828.
38 W. Liang, P. M. Bhatt, A. Shkurenko, K. Adil, G. Mouchaham, H. Aggarwal, A. Mallick, A. Jamal, Y. Belmabkhout and M. Eddaoudi, *Chem*, 2019, **5**, 950–963.
39 N. Li, Z. Chang, H. Huang, R. Feng, W. W. He, M. Zhong, D. G. Madden, M. J. Zaworotko and X. H. Bu, *Small*, 2019, **15**, 1900426.

40 E. Martínez-Ahumada, M. L. Díaz-Ramírez, H. A. Lara-García, D. R. Williams, V. Martis, V. Jancik, E. Lima and I. A. Ibarra, *J. Mater. Chem. A*, 2020, **8**, 11515–11520.
41 T. Islamoglu, Z. Chen, M. C. Wasson, C. T. Buru, K. O. Kirlikovali, U. Afrin, M. R. Mian and O. K. Farha, *Chem. Rev.*, 2020, **120**, 8130–8160.
42 Y. Chen, Y. Du, P. Liu, J. Yang, L. Li and J. Li, *Environ. Sci. Technol.*, 2020, **54**, 3636–3642.
43 C. Lu, Y. Chen, Y. Wang, Y. Du, J. Yang, L. Li and J. Li, *Sep. Purif. Technol.*, 2022, **282**, 120126.
44 T. Asefa, K. Koh and C. W. Yoon, *Adv. Energy Mater.*, 2019, **9**, 1901158.
45 U. Eberle, M. Felderhoff and F. Schuth, *Angew. Chem., Int. Ed.*, 2009, **48**, 6608–6630.
46 X. Liang, P. Wang, C. Li, M. Yuan, Q. Shi and J. Dong, *Microporous Mesoporous Mater.*, 2021, **320**, 111109.
47 C. Jia, F. G. Cirujano, B. Bueken, B. Claes, D. Jonckheere, K. M. Van Geem and D. De Vos, *ChemSusChem*, 2019, **12**, 1256–1266.
48 C. Wang, Y. H. Luo, X. T. He, D. L. Hong, J. Y. Wang, F. H. Chen, C. Chen and B. W. Sun, *Inorg. Chem.*, 2019, **58**, 3058–3064.
49 Y. Yan, I. da Silva, A. J. Blake, A. Dailly, P. Manuel, S. Yang and M. Schröder, *Inorg. Chem.*, 2018, **57**, 12050–12055.
50 X. Wu, L. Peng, S. Xiang and W. Cai, *Phys. Chem. Chem. Phys.*, 2018, **20**, 30150–30158.
51 Z. H. Zhang, H. Fang, D. X. Xue and J. Bai, *ACS Appl. Mater. Interfaces*, 2021, **13**, 44956–44963.
52 Y. Peng, V. Krungleviciute, I. Eryazici, J. T. Hupp, O. K. Farha and T. Yildirim, *J. Am. Chem. Soc.*, 2013, **135**, 11887–11894.
53 J. Jiang, H. Furukawa, Y. B. Zhang and O. M. Yaghi, *J. Am. Chem. Soc.*, 2016, **138**, 10244–10251.
54 M. Zhang, W. Zhou, T. Pham, K. A. Forrest, W. Liu, Y. He, H. Wu, T. Yildirim, B. Chen, B. Space, Y. Pan, M. J. Zaworotko and J. Bai, *Angew. Chem., Int. Ed.*, 2017, **56**, 11426–11430.
55 B. Li, H. M. Wen, H. Wang, H. Wu, M. Tyagi, T. Yildirim, W. Zhou and B. Chen, *J. Am. Chem. Soc.*, 2014, **136**, 6207–6210.
56 J. Lin, C. He, Y. Liu, P. Liao, D. Zhou, J. Zhang and X. Chen, *Angew. Chem., Int. Ed.*, 2016, **55**, 4674–4678.
57 B. Li, H. Wen, H. Wang, H. Wu, T. Yildirim, W. Zhou and B. Chen, *Energy Environ. Sci.*, 2015, **8**, 2504–2511.
58 S. Ma, D. Sun, J. Simmons, C. Collier, D. Yuan and H. Zhou, *J. Am. Chem. Soc.*, 2007, **130**, 1012–1016.
59 J. Wang, Y. Zhang, Y. Su, X. Liu, P. Zhang, R. B. Lin, S. Chen, Q. Deng, Z. Zeng, S. Deng and B. Chen, *Nat. Commun.*, 2022, **13**, 200.
60 J. Pei, J. Wang, K. Shao, Y. Yang, Y. Cui, H. Wu, W. Zhou, B. Li and G. Qian, *J. Mater. Chem. A*, 2020, **8**, 3613–3620.
61 L. Li, H. M. Wen, C. He, R. B. Lin, R. Krishna, H. Wu, W. Zhou, J. Li, B. Li and B. Chen, *Angew. Chem., Int. Ed.*, 2018, **57**, 15183–15188.
62 H. Wang, Z. Shi, J. Yang, T. Sun, B. Rungtaweevoranit, H. Lyu, Y. B. Zhang and O. M. Yaghi, *Angew. Chem., Int. Ed.*, 2021, **60**, 3417–3421.
63 B. Li, X. Cui, D. O'Nolan, H. M. Wen, M. Jiang, R. Krishna, H. Wu, R. B. Lin, Y. S. Chen, D. Yuan, H. Xing, W. Zhou, Q. Ren, G. Qian, M. J. Zaworotko and B. Chen, *Adv. Mater.*, 2017, **29**, 1704210.
64 H. Wen, L. Li, R. Lin, B. Li, B. Hu, W. Zhou, J. Hu and B. Chen, *J. Mater. Chem. A*, 2018, **6**, 6931–6937.
65 Q. Qian, X. Gu, J. Pei, H. Wen, H. Wu, W. Zhou, B. Li and G. Qian, *J. Mater. Chem. A*, 2021, **9**, 9248–9255.
66 J. Li, L. Jiang, S. Chen, A. Kirchon, B. Li, Y. Li and H. C. Zhou, *J. Am. Chem. Soc.*, 2019, **141**, 3807–3811.
67 F. Zheng, L. Guo, B. Gao, L. Li, Z. Zhang, Q. Yang, Y. Yang, B. Su, Q. Ren and Z. Bao, *ACS Appl. Mater. Interfaces*, 2019, **11**, 28197–28204.
68 J. Pei, K. Shao, J. X. Wang, H. M. Wen, Y. Yang, Y. Cui, R. Krishna, B. Li and G. Qian, *Adv. Mater.*, 2020, **32**, 1908275.
69 T. Ke, Q. Wang, J. Shen, J. Zhou, Z. Bao, Q. Yang and Q. Ren, *Angew. Chem., Int. Ed.*, 2020, **59**, 12725–12730.
70 S. Chu, Y. Cui and N. Liu, *Nat. Mater.*, 2016, **16**, 16–22.
71 H. Wang, X. Dong, V. Colombo, Q. Wang, Y. Liu, W. Liu, X. L. Wang, X. Y. Huang, D. M. Proserpio, A. Sironi, Y. Han and J. Li, *Adv. Mater.*, 2018, **30**, 1805088.
72 D. Lv, P. Zhou, J. Xu, S. Tu, F. Xu, J. Yan, H. Xi, W. Yuan, Q. Fu, X. Chen and Q. Xia, *Chem. Eng. J.*, 2022, **431**, 133208.
73 X. Wang, Z. Niu, A. M. Al-Enizi, A. Nafady, Y. Wu, B. Aguila, G. Verma, L. Wojtas, Y. Chen, Z. Li and S. Ma, *J. Mater. Chem. A*, 2019, **7**, 13585–13590.
74 P. Zhou, L. Yue, X. Wang, L. Fan, D. L. Chen and Y. He, *ACS Appl. Mater. Interfaces*, 2021, **13**, 54059–54068.
75 A. Schneemann, Y. Jing, J. D. Evans, T. Toyao, Y. Hijikata, Y. Kamiya, K. I. Shimizu, N. C. Burtch and S. I. Noro, *Dalton Trans.*, 2021, **50**, 10423–10435.
76 H. Yang, Y. Wang, R. Krishna, X. Jia, Y. Wang, A. N. Hong, C. Dang, H. E. Castillo, X. Bu and P. Feng, *J. Am. Chem. Soc.*, 2020, **142**, 2222–2227.
77 Y. Wang, C. Hao, W. Fan, M. Fu, X. Wang, Z. Wang, L. Zhu, Y. Li, X. Lu, F. Dai, Z. Kang, R. Wang, W. Guo, S. Hu and D. Sun, *Angew. Chem., Int. Ed.*, 2021, **60**, 11350–11358.
78 K. B. Idrees, Z. Chen, X. Zhang, M. R. Mian, R. J. Drout, T. Islamoglu and O. K. Farha, *Chem. Mater.*, 2020, **32**, 3776–3782.
79 A. P. Ladshaw, A. I. Wiechert, A. K. Welty, K. L. Lyon, J. D. Law, R. T. Jubin, C. Tsouris and S. Yiacoumi, *Chem. Eng. J.*, 2019, **375**, 122073.
80 X. Xiong, G. Chen, S. Xiao, Y. Ouyang, H. Li and Q. Wang, *J. Phys. Chem. C*, 2020, **124**, 14603–14612.
81 J. Qian, G. Chen, S. Xiao, H. Li, Y. Ouyang and Q. Wang, *RSC Adv.*, 2020, **10**, 17195–17204.
82 H. Zhang, Y. Fan, R. Krishna, X. Feng, L. Wang and F. Luo, *Sci. Bull.*, 2021, **66**, 1073–1079.
83 T. Wang, Y. L. Peng, E. Lin, Z. Niu, P. Li, S. Ma, P. Zhao, Y. Chen, P. Cheng and Z. Zhang, *Inorg. Chem.*, 2020, **59**, 4868–4873.
84 Q. Wang, T. Ke, L. Yang, Z. Zhang, X. Cui, Z. Bao, Q. Ren, Q. Yang and H. Xing, *Angew. Chem., Int. Ed.*, 2020, **59**, 3423–3428.